Directing cellular information flow via CRISPR signal conductors

Yuchen Liu, Yonghao Zhan, Zhicong Chen, Anbang He, Jianfa Li, Hanwei Wu, Li Liu, Chengle Zhuang, Junhao Lin, Xiaoqiang Guo, Qiaoxia Zhang, Weiren Huang & Zhiming Cai

The complex phenotypes of eukaryotic cells are controlled by decision-making circuits and signaling pathways. A key obstacle to implementing artificial connections in signaling networks has been the lack of synthetic devices for efficient sensing, processing and control of biological signals. By extending sgRNAs to include modified riboswitches that recognize specific signals, we can create CRISPR–Cas9-based 'signal conductors' that regulate transcription of endogenous genes in response to external or internal signals of interest. These devices can be used to construct all the basic types of Boolean logic gates that perform logical signal operations in mammalian cells without needing the layering of multiple genetic circuits. They can also be used to rewire cellular signaling events by constructing synthetic links that couple different signaling pathways. Moreover, this approach can be applied to redirect oncogenic signal transduction by controlling simultaneous bidirectional (ON–OFF) gene transcriptions, thus enabling reprogramming of the fate of cancer cells.

© 2016 Nature America, Inc. All rights reserved.

Living organisms transduce signals into appropriate cellular responses[1–3]. To investigate the design principles of signals that achieve complex responses, biologists have created various systems[4] ranging from biological information processing circuits[5,6] to reconstructed gene regulatory networks[7,8]. These biological systems have been used to link the detection of cellular state and environmental signals to artificial control of downstream genes. Previous approaches to circuit engineering have relied on small-molecule or light-responsive devices, engineered DNA-binding proteins and so on[5–8], which may require multiple processes to construct and optimize function. Thus, implementation of the designed communications in endogenous networks through simple engineering remains a challenge. Development of devices which serve to integrate information from many unrelated biomolecules would be key to addressing this problem, but few studies have attempted to resolve this issue so far.

The CRISPR–Cas9 system provides a powerful tool for genome editing and gene regulation across various organisms[9–15]. However, the engineering of endogenous gene networks remains limited by the inability of Cas9 to interface with various biological signals. To repurpose this system for signal control and assignment, we constructed a platform that combines ligand-responsive riboswitches and single guide RNAs (sgRNAs) to create a newly engineered class of devices, which we call signal conductors.

RESULTS

Construction of CRISPR–Cas9-based signal conductors

We have developed Cas9-based signal conductors that create a synthetic link to control endogenous proteins and RNAs. We reengineered the sgRNA by integrating a previously characterized signal-responsive aptamer[16], thus linking signal concentrations to gene-expression events. In theory, one CRISPR–Cas9-based device can inactivate or activate the transcription of any gene of interest in response to any signal, and it can function as a signal conductor. The redesigned sgRNA uses the traditional module to recruit the transcriptional repressor (catalytically inactive Cas9) or activator (dCas9–VP64 fusion protein) and the riboswitch module to recognize a specific signal (**Fig. 1a**,**b**). In the absence of the specific signal, the guide region of the original sgRNA is paired with the designed antisense stem and cannot bind to its target DNA. One specific signal A (or B) can bind to the aptamer and induce a conformational change that allows the guide region of sgRNA to interact with the corresponding DNA sequence to affect transcription of another signal B (or A). This approach converts the traditional sgRNA into a scaffold RNA that couples the detection of one input signal with the production of another output signal.

Control of endogenous gene expression

We tested whether an external signal can affect the transcription of a non-native downstream gene encoding VEGF protein in HEK-293T cells (**Fig. 2a** and **Supplementary Table 1**). We incorporated a tetracycline aptamer[17] into the 3′ end of each of the four effective sgRNAs (**Supplementary Fig. 1a**). The aptamer stem was modified to base pair with the guide region of sgRNA. We varied the lengths of the antisense stem and found that the optimal stem length was 15 bp. Increasing the length of the optimal stem could result in lower repression efficiency, whereas decreasing the length generated sgRNAs that inhibited

State Engineering Laboratory of Medical Key Technologies Application of Synthetic Biology, Shenzhen Second People's Hospital, the First Affiliated Hospital of Shenzhen University, Shenzhen, China. Correspondence should be addressed to W.H. (pony8980@163.com) or Z.C. (caizhiming2000@163.com).

RECEIVED 21 MARCH; ACCEPTED 8 AUGUST; PUBLISHED ONLINE 5 SEPTEMBER 2016; DOI:10.1038/NMETH.3994

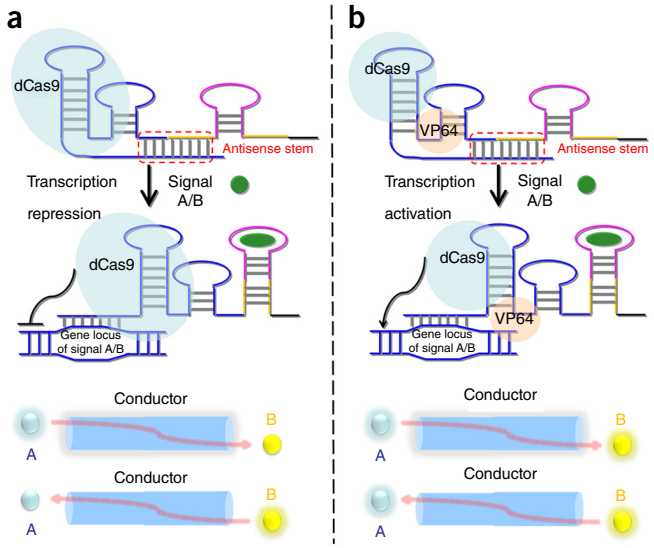


Figure 1 | Design of the CRISPR–Cas9-based signal conductor that links one signal with another. General illustration of the strand-displacement mechanisms by which the redesigned sgRNAs acts to inactivate (**a**) or activate (**b**) gene expression. The antisense sequence of the sgRNA is shown in blue, and the aptamer stem is shown in yellow. In the absence of signal A (B), the guide region of sgRNA is paired within the antisense stem and the sgRNA is in the 'off' state. In the presence of signal A (B), the conformation of the redesigned sgRNA is switched to the 'on' state. In this state, the guide region of the sgRNA binds to its target DNA and thus turns the production of signal B (A) on and off through the dCas9–VP64 fusion protein and the dCas9 protein, respectively.

VEGF expression without tetracycline (**Supplementary Fig. 2a**,**b**). Each optimized sgRNA–dCas9 (**Supplementary Table 2**) showed an efficient silencing effect in the presence of 50 μM tetracycline (**Supplementary Fig. 3a**). We saw a dose-dependent repressive effect upon treatment with tetracycline (**Fig. 2b**). The optimized sgRNAs bearing riboswitches at the 3′ end retained most of their functionalities (**Supplementary Fig. 1a**).

To determine whether the signal conductors activated transcription in response to tetracycline, we coexpressed dCas9–VP64 and reprogrammed sgRNA and examined the induced effects using HEK-293T. After the addition of 50 μM tetracycline, all four optimized sgRNAs (**Supplementary Fig. 4a**,**b** and **Supplementary Table 2**) induced significant increases in *VEGF* mRNA (**Supplementary Table 1**) and protein expression when combined with dCas9–VP64 (**Supplementary Fig. 3b**). We also generated dose–response curves and saw results similar to those in **Figure 2b** (**Fig. 2c**). Consistently, changes in gene activation induced by each pair of sgRNAs were indistinguishable, indicating that the riboswitches didn't obviously alter dCas9–VP64/sgRNA activity (**Supplementary Fig. 1b**).

We then replaced the tetracycline aptamer with theophylline aptamer[17] (**Supplementary Table 2**), leaving stem sequence identical to the previous design. To test whether the length of antisense stem affected the abilities of these sgRNAs, we generated constructs containing stems of various lengths. Four optimized sgRNAs, each harboring a 15-bp stem, were selected for the following experiments according to their activities with and without theophylline (**Supplementary Figs. 5a**,**b** and **6a**,**b**). Similar repression and activation effects were observed when each optimized sgRNA was coexpressed with the dCas9 and dCas9–VP64, respectively (**Supplementary Fig. 7a**,**b**). The theophylline-responsive devices demonstrated dynamic ranges in response to higher input concentrations relative to the tetracycline-responsive devices (**Supplementary Fig. 7c**,**d**). We also confirmed that riboswitches at the 3′ end of reprogrammed sgRNAs still resulted in no significant loss of dCas9–sgRNA or dCas9–VP64/sgRNA activities (**Supplementary Fig. 7e**,**f**).

To further determine whether the signal conductors influenced transcription in response to intracellular protein, we introduced the aptamer for the bacteriophage coat protein MS2 (ref. 18) into the related region of sgRNA (**Supplementary Table 2**). We selected two noncoding genes (*MALAT1* and *UCA1*) as the targets and analyzed the dynamic responses of these devices using HEK-293T cells that stably expressed the tetracycline controlled (tet-on) MS2-inducible system. In the presence of doxycycline (Dox), the synthetically introduced MS2 protein was induced at the concentrations of 0.1–2 μg/mL in a dose-dependent manner (**Supplementary Fig. 8**). Although there were some quantitative differences from the activity trends observed in small-molecule-induced sgRNAs, the optimal length of antisense stem was still 15 bp, indicating a general pattern for designing reprogrammed sgRNAs (**Supplementary Figs. 9–12**). Each of these optimized devices displayed tetracycline-responsive regulation over a range of input concentrations (**Fig. 2d–g**). Negative controls with mutant aptamers (**Supplementary Table 3**) showed that these responses were specific to the sgRNAs containing wildtype aptamers. Additional assays on activity of the devices indicated that the reprogrammed sgRNAs retained their normal abilities to regulate transcription compared with the original sgRNAs (**Supplementary Fig. 13a–d**). The complete design process for reprogrammed sgRNAs is summarized in **Supplementary Figure 14**.

Construction of Boolean logic gates

According to the regulatory property of the signal conductors, we constructed various logic gates[19] in which signals could be combined to make a decision (**Fig. 3a**). By integrating different combinations of reprogrammed sgRNAs (**Supplementary Table 4**), we built all the basic types of Boolean logic gates in HEK-293T cells stably expressing Renilla luciferase. We integrated the modified aptamer recognizing endogenous p53 (ref. 20) or HSF-1 (ref. 21) signal into the 3′ end of each sgRNA targeting Renilla luciferase, such that these gates could use p53 and HSF1 as the input signals and operate with the output luciferase signal. To activate the expression of the endogenous p53, we chose Tenovin-6, a small chemical molecule, to elevate the protein level of p53. The cellular expression of p53 was strikingly increased by Tenovin-6 in a dose-dependent manner (**Supplementary Fig. 15a**). Using ethanol as the other trigger, HSF1 protein expression was induced in an ethanol-dependent manner (**Supplementary Fig. 15b**).

First, we constructed two NOT gates that exhibited high output only when the input signal was absent. We designed several original sgRNAs to cover the luciferase coding sequence or the promoter region, and most of them repressed luciferase expression to some extent (**Supplementary Fig. 16a**,**b**). Two original sgRNAs with high repression efficiencies in the presence of dCas9 were used to construct the reprogrammed sgRNAs that formed the NOT gates, and the extended riboswitches did not lose the gene regulatory activities of sgRNAs (**Supplementary**

© 2016 Nature America, Inc. All rights reserved.

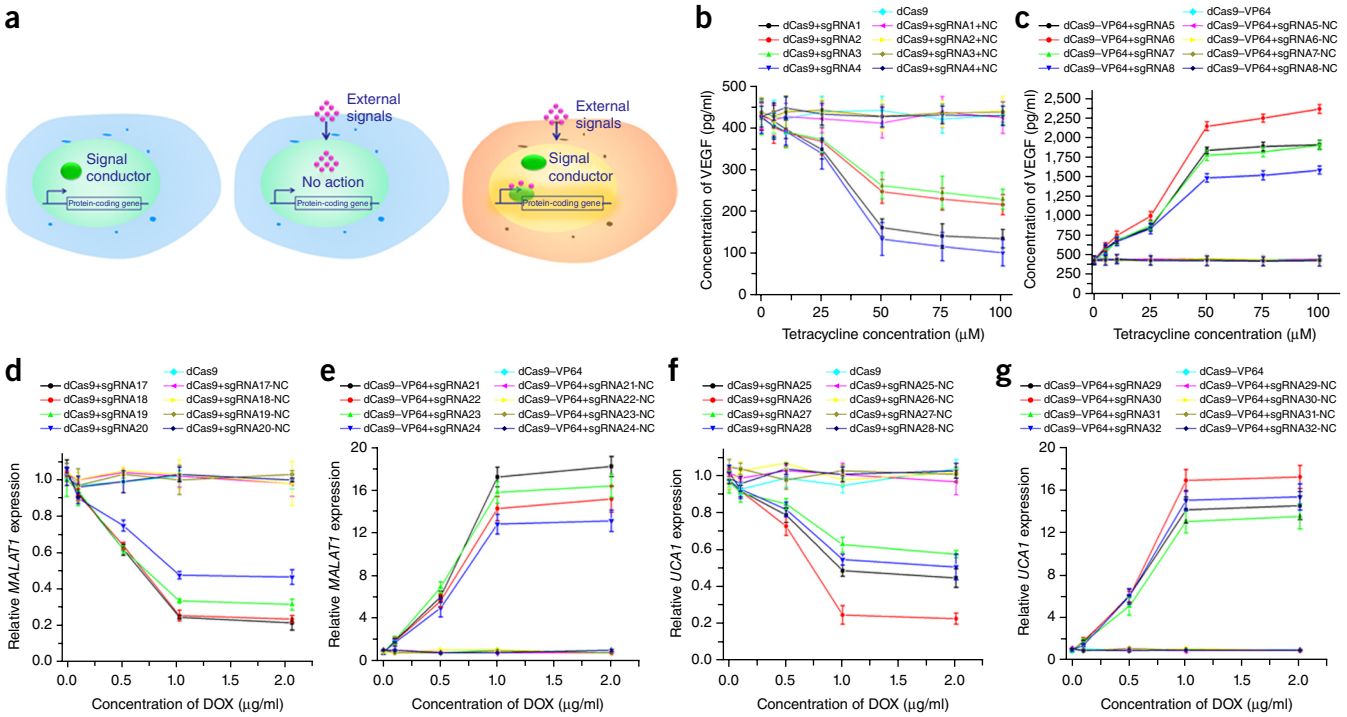


Figure 2 | Ligand-regulated transcriptional activation or inactivation. (**a**) The signal conductor links the presence of external drug to the transcription of a non-native target gene. (**b**) *In vivo VEGF* regulatory activity of the engineered devices responsive to tetracycline across different concentrations. The error bars indicate the s.d. from five different experiments. NC, negative control. (**c**) Effect of tetracycline concentration on Cas9-dependent *VEGF* activation. The error bars indicate the s.d. from five different experiments. The relative RNA levels of *MALAT1* (**d** and **e**) and *UCA1* (**f** and **g**) are shown for the signal conductors at various Dox concentrations. The error bars indicate the s.d. from five different experiments.

© 2016 Nature America, Inc. All rights reserved.

Fig. 16c). Only in the absence of corresponding trigger did each NOT gate produce high luciferase output (**Fig. 3b**). In contrast, exposure of cells to increasing concentrations of Tenovin-6 or ethanol dramatically decreased luciferase mRNA expression (**Supplementary Table 1**).

Using similar approaches, we then confirmed that the devices could function as AND (**Supplementary Fig. 17**), NAND (**Supplementary Fig. 18**), OR (**Supplementary Fig. 19**), NOR (**Supplementary Fig. 20**), XOR (**Supplementary Fig. 21**) and XNOR (**Supplementary Fig. 22**) gates (**Supplementary Fig. 23**). Logic gate controls with mutant aptamers (**Supplementary Table 3**) showed that the logic responses were specific to the wildtype aptamers (**Supplementary Fig. 24a–g**).

Artificial networks connecting two signaling pathways

Because signal conductors could effectively produce a novel linkage between two specific signals, we then asked whether they could redirect the output responses of native signaling pathways by establishing artificial networks (**Fig. 3c**). We designed two types of artificial connections between β-catenin and NF-κB. In this design, activation of β-catenin caused upregulation of the NF-κB signaling pathway, while the latter inhibited the activity of β-catenin (**Fig. 3c**). We inserted modified β-catenin or NF-κB aptamers[18] into the 3′ end of each sgRNA containing the designed 15-bp antisense stem for recognizing NF-κB (p65) or β-catenin (CTNNB1), and we expressed dCas9 or dCas9–VP64 in human bladder cancer T24 cells, which highly expressed both NF-κB and β-catenin proteins (**Supplementary Fig. 25**). The two reprogrammed sgRNAs (**Supplementary Table 2**) were shown to regulate *β-catenin* (*CTNNB1*) and *NF-κB* (*REL-A*) directly when the signaling pathways were stimulated (**Supplementary Fig. 26a**,**b**). To further evaluate whether a β-catenin-responsive device could increase NF-κB signaling, we then examined the transcription of known NF-κB targets. The mRNA expression levels of two genes downstream of β-catenin (*DPAGT1* and *APCDD1*; **Supplementary Table 1**) were elevated when cells were treated with LTD4, an activator of β-catenin. Compared with dCas9–VP64 or a control device containing mutant aptamer (**Supplementary Table 3**), the signal conductor obviously increased the mRNA levels of genes downstream of NF-κB (*BFL1* (*BCL2A1*) and *MET*; **Supplementary Table 1**) in response to LTD4 (**Fig. 3d**). To further ensure that the observed changes were caused by activation of NF-κB, we also treated cells with NF-κB small hairpin RNA (shRNA). This shRNA largely reversed the upregulation of NF-κB downstream genes mediated by signal conductor (**Supplementary Fig. 27a**,**b**). We then examined the effects of stimulating the NF-κB pathway with TNF-α on the expression of *BFL1* and *MET*. The two genes were robustly activated by TNF-α in cells expressing the signal conductor or the negative controls. In comparison, only cells expressing the signal conductor displayed decreased expressions of *DPAGT1* and *APCDD1* (**Fig. 3e**). Overexpression of β-catenin ablated these effects (**Supplementary Fig. 27c**,**d**).

Redirecting oncogenic signaling to an antioncogenic pathway

One hypothetical use of the signal conductors is to create connections that link oncogenic signals with activation of antioncogenic genes. Nucleophosmin (NPM)[22] is an oncogenic signal that activates the MAPK pathway and promotes cell proliferation

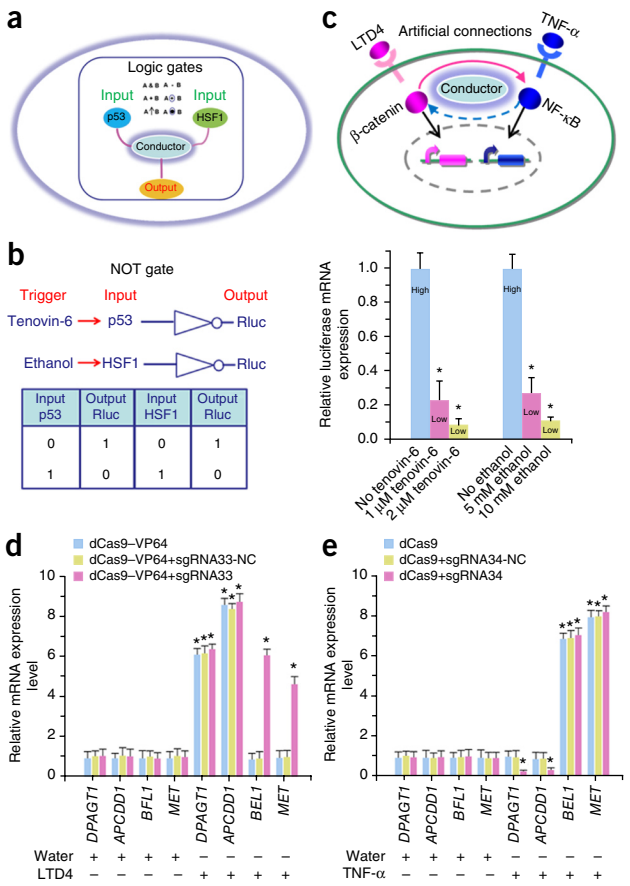


Figure 3 | Logic connections were constructed using the signal conductors in HEK-293T cells. (**a**) Description of a logic gate and (**b**) NOT gate. Device responses under different trigger concentrations are represented as the relative mRNA level of Renilla luciferase (Rluc) at 48 h after transient transfection of dCas9 (or dCas9–VP64) and each sgRNA. Error bars represent the s.d. from five independent experiments. *P < 0.05, relative to the blank control by paired, one-sided t-test. (**c**) Artificial connections were generated between the β-catenin signaling pathway and the NF-κB signaling pathway through the signal conductor. (**d**) Changes in relative expression levels of the downstream genes of the β-catenin–NF-κB signaling pathway in T24 cells treated with LTD4 and the signal conductors. Error bars represent the s.d. from five independent experiments. *P < 0.05, compared with the dCas9 control or the corresponding sgRNA negative control by paired, one-sided t-test. (**e**) Changes in relative expression levels of the downstream genes of the two signaling pathways in T24 cells treated with TNF-α and the engineered devices. Error bars represent the s.d. from five independent experiments. *P < 0.05, compared with the dCas9 control or the corresponding sgRNA negative control by paired, one-sided t-test.

in progression of bladder cancer[23] (**Fig. 4a**). We rewired NPM signaling from the proliferation pathway to quiescence in bladder cancer by constructing a signal conductor that activated the transcription of two tumor suppressors (*P53* (*TP53*) and *P21* (*CDKN1A*)) in response to cellular NPM proteins. We inserted the designed antisense region and modified NPM aptamer[22] into sgRNAs targeting *P53* and *P21* (**Supplementary Table 2**) and expressed dCas9–VP64 in T24 cells. Compared with negative controls containing mutant aptamers (**Supplementary Table 3**), the signal conductor obviously increased the expression levels of both *P53* and *P21* (**Supplementary Fig. 28a–c**). Inhibition of cell growth was observed in the group transfected with signal conductor (**Fig. 4b**), and knockdown of NPM (**Supplementary Fig. 28d**) ablated this effect. Furthermore, either shRNA-p53 or shRNA-p21 (**Supplementary Fig. 28e,f**) was able to partly reverse this inhibition of cell proliferation, indicating that the signal conductor executed its function by activating *P53* and *P21*.

Ets-1 is another oncogenic signal which activates the transcription of matrix metalloproteases (MMPs) and promotes cell migration in bladder cancer cells[24]. We rewired Ets-1 signaling from the migration pathway to quiescence in bladder cancer by constructing a signal conductor that activated the transcription of one tumor migration suppressor (E-cadherin) in response to Ets-1 (**Fig. 4a**). We inserted modified Ets-1 aptamer[24] into the *E-cadherin* (*CDH1*) sgRNA containing a 15-bp antisense stem recognizing Ets-1 signals (**Supplementary Table 2**) and expressed dCas9–VP64 in T24 cells. The signal conductor obviously increased both the mRNA and protein levels of *E-cadherin* (**Supplementary Fig. 29a,b** and **Supplementary Table 1**). Inhibition of cell migration was observed in the group transfected with signal conductor (**Fig. 4c**), and knockdown of Ets-1 (**Supplementary Fig. 29c**) ablated this effect. As expected, shRNA-E-cadherin (**Supplementary Fig. 29d**) was able to partly reverse this inhibition of cell migration, indicating that the signal conductor executed its function by activating *E-cadherin*.

Simultaneous activation and repression of genes

To simultaneously induce gene activation and repression, we generated an alternative sgRNA design in which stem loops 2 and 3 of the sgRNA were replaced by the MS2 or Rev aptamer[25] (**Supplementary Table 2**). We speculated that this alternative design may enable simultaneous activation and repression of endogenous genes when the MS2–dCas9 and Rev–dCas9–VP64 were coexpressed within a single cell (**Fig. 5a**). To test this design, we selected the protein-coding genes *BAX* and *BCL2* as the targets of the reprogrammed sgRNAs and chose alpha-fetoprotein (AFP) as the oncogenic signal, which forced the antisense stem of sgRNA containing AFP aptamer[26] into a single-stranded state. Since the ratio of Bcl2 to Bax is closely associated with the sensitivity of cells to apoptosis[27], we constructed reprogrammed sgRNAs to repress *BCL2* with MS2–dCas9 and to activate *BAX* with Rev–dCas9–VP64 in human liver cancer HepG2 cells which possessed a high level of AFP. A 15-bp antisense stem was also found to be optimal for this new type of reprogrammed sgRNAs (**Supplementary Fig. 30a,b**). The treated HepG2 cells showed a decrease in *BCL2* expression and an increase in *BAX* expression with the optimized signal conductor (**Fig. 5b**). We also confirmed the related expression changes at the protein levels (**Supplementary Fig. 30c**) and showed that these effects were dependent on MS2 or Rev that fused to dCas9 (**Supplementary Fig. 30d**). In contrast, the expression of these two genes was not changed by the device in the AFP-negative normal hepatic cell line WRL-68. We then examined whether apoptosis of HepG2 cells could be induced by the signal conductor (**Fig. 5c**). Compared to the negative control containing the mutant aptamer (**Supplementary Table 3**), cells transiently transfected with the signal conductor exhibited stronger blue fluorescence, revealing typical apoptotic characteristics. Knockdown of AFP by shRNA (**Supplementary Fig. 30e**) ablated these effects. The control devices (MS2–dCas9+sgRNA38 or Rev–dCas9–VP64+sgRNA39), which activated *BAX* expression or repressed *BCL2* expression alone, didn't increase the apoptotic rate of HepG2 cells.

© 2016 Nature America, Inc. All rights reserved.

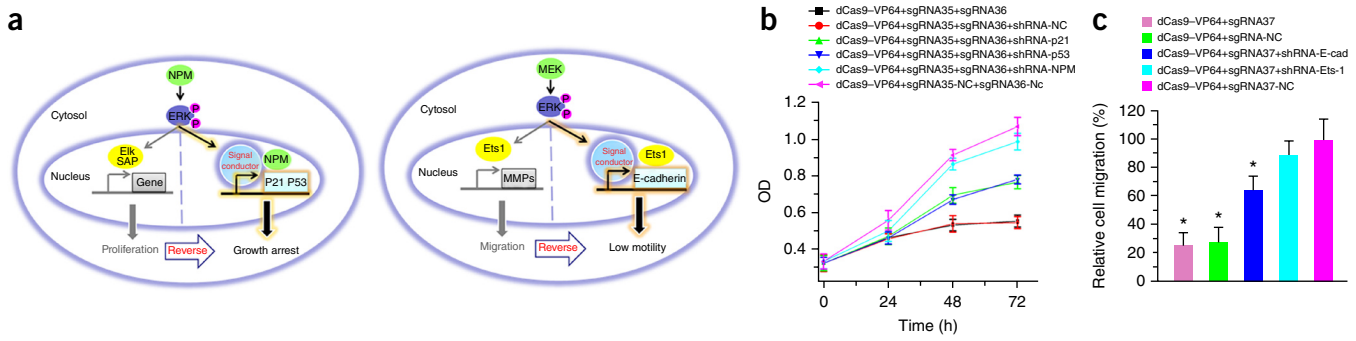


Figure 4 | The CRISPR–Cas9-based signal conductors redirect the oncogenic signaling to the antioncogenic pathway. (**a**) The oncogenic signals NPM and Ets1 were used to promote the accumulation of two antioncogenic signals, p21 and p53, by the signal conductor in cancer cells. Schematics of two rewired oncogenic pathways. (**b**) Cell proliferation changes caused by transient transfection of the signal conductor or one of the controls. Error bars represent the s.d. from five independent experiments. OD, optical density. (**c**) Cell motility changes caused by transient transfection of the signal conductor or the controls. Error bars represent the s.d. from five independent experiments. $*P < 0.05$, compared with the negative control by paired, one-sided *t*-test.

To integrate multiple signals, we then constructed a two-input AND gate that used two oncogenic signals as the inputs and had a high output only if both inputs were high. We determined the expression patterns of NF-κB and β-catenin in several cancer cell lines (T24, HepG2 and ACHN) and normal cell lines (SV-HUC1, HEK-293T and WRL-68), all of which were engineered to stably express GFP. The results showed that NF-κB and β-catenin were both highly expressed in the three cancer cell lines but not in the normal cell lines (**Supplementary Fig. 25**) with which the cancer cells lines were compared. By combining these two input signals into the design, we tested whether the AND gate circuit could have a strong ability to selectively and effectively influence cancer cells (**Fig. 6a**). A programmed sgRNA (sgRNA-40) recognizing NF-κB was used to suppress *BCL2*, and a programmed sgRNA recognizing β-catenin (sgRNA-41) was constructed to activate *BAX* expression (**Supplementary Table 2**). The anticancer ability of the AND gate was then determined by measuring the inhibition of GFP intensity in cells treated with the signal conductor or controls. GFP intensity as an indicator of survival of device-treated cells was determined and compared with that of cells transfected with a negative control containing the mutant aptamer (**Supplementary Table 3**). The signal conductor was able to reduce GFP intensity only in the cancer cells, and knockdown of NF-κB or Bcl2 (**Supplementary Fig. 31a–f**) partly reversed the induced GFP-decreasing effects (**Supplementary Fig. 32a,b**). Although the signal conductor had no such effects in normal cell lines, reduced GFP intensity could be observed when the missing protein was re-expressed (**Supplementary Fig. 32a,b** and **Supplementary Fig. 33a–f**). Cell apoptosis was further quantitatively determined (**Fig. 6b,c**), and this analysis showed that the signal conductor selectively triggered apoptosis in cancer cells without affecting the normal cells. Perturbation of β-catenin and NF-κB could alter the corresponding effects. Finally, we examined the anticancer effect of this circuit on *in vivo* tumor development. The cancer cells were subcutaneously injected into female nude mice, and tumors developed several days after cell inoculation. The therapeutic ability of the circuit was tested by direct intratumoral injection of circuit-expressing plasmids. The sizes of tumors treated with the AND gate circuit were dramatically smaller than those treated with the negative control mutant (**Supplementary Table 3**). The average tumor weight was markedly lower in the circuit-treated group compared with that in the negative control group at the end of the experiment (**Supplementary Fig. 34**).

DISCUSSION

A wide range of artificial RNA-based switches have emerged for construction of genetic circuits, such as RNAi-based regulators[28,29], programmable riboswitches[30,31], ligand-responsive

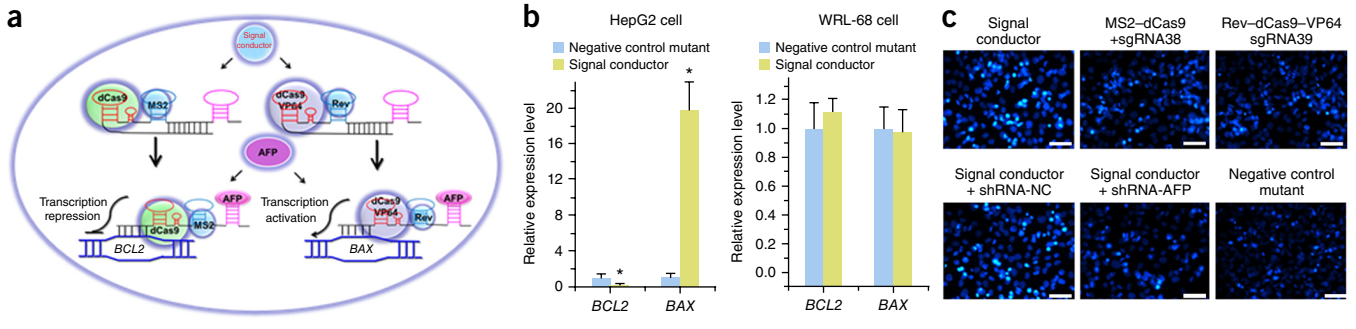


Figure 5 | The CRISPR–Cas9-based signal-conductor induces simultaneous activation and repression of cellular genes in response to oncogenic signals. (**a**) sgRNA constructs with MS2 or Rev RNA hairpins recruit their cognate RNA-binding proteins fused to dCas9 or dCas9–VP64 to activate or repress target gene transcription within the same cell. (**b**) Changes in relative expression levels of *BCL2* and *BAX* after transient transfection of the signal conductor or one of the controls. Error bars represent the s.d. from five independent experiments. $*P < 0.05$ compared with the negative control containing mutated aptamer by paired, one-sided *t*-test. (**c**) Cell apoptosis was measured by Hoechst 33258 staining at 48 h after transient transfection, and representative images are shown. Scale bars, 50 μm in each figure.

© 2016 Nature America, Inc. All rights reserved.

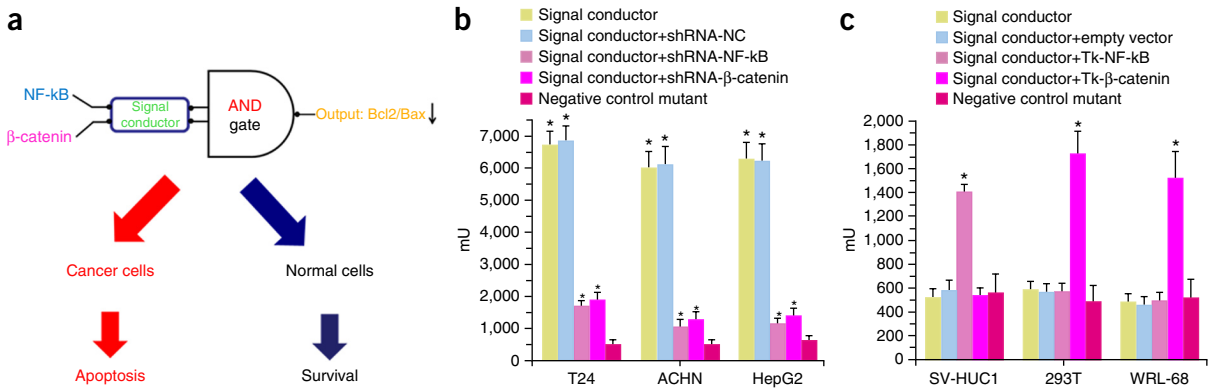


Figure 6 | Apoptosis levels of several cell lines treated with the AND gate circuit. (**a**) Schematic representations of the synthetic circuit based on the signal conductor. (**b**,**c**) Changes in the level of apoptosis in cells transfected with the AND gate circuit. mU, absorbance (10^{-3}). Error bars represent the s.d. from five independent experiments. *$P < 0.05$, relative to the negative control mutant by paired, one-sided *t*-test.

ribozyme switches[32,33] and CRISPR–Cas transcription factors (CRISPR–TFs)[11–13]. Each of these devices has its own advantages and disadvantages. CRISPR–TFs[11–13] inhibit or activate endogenous gene expression, and the reprogrammed sgRNAs that recruit effector proteins to a different target locus can rewire the yeast metabolic pathway. Even so, previously developed CRISPR–TFs can't respond to a variety of signals, leaving a large amount of biological information inaccessible.

Although Shechner *et al.*[34] successfully connected noncoding RNAs with unrelated genome loci through the strategy 'CRISPR-Display', this is the first description of the use of riboswitch-based CRISPR to integrate information about different biomolecules. These signal conductors allowed highly responsive, dose-dependent and dynamic control of gene expression. The performance of one signal conductor mainly depends on two factors: the sgRNA guide region that binds to a specific DNA target and the length of the sgRNA antisense stem. There should be a correlation between the RNA free energies and the device performance. The lower efficiency of one sgRNA with a longer antisense stem was presumed to be due to the more stable secondary structure shaped by the stem. Conversely, the higher 'leakage' from one sgRNA with a shorter antisense stem was hypothesized to be due to the lower stability of the strand hybrids. Although a 15-bp antisense stem was found to be optimal across all reprogrammed sgRNAs, aptamers with vastly different binding affinities may also result in different optimal lengths. ΔΔG between the induced and basal states and the quantitative relationship between the energetics of the strand switching and the performance of these devices require further studies.

Subsequent preclinical studies demonstrated that intratumoral injection of plasmids expressing signal conductors slowed development of subcutaneous tumors, although naked plasmids had no penetration beyond the injection area. It would be possible to treat solid organ tumors using these devices once problems such as efficient *in vivo* gene delivery are overcome. Future therapeutic studies must focus on other issues, such as increasing many more negative controls, investigating cell-to-cell variability and resolving tumor heterogeneity.

In this study, truncated sgRNAs containing heterologous protein aptamers could be used to target gene expression when the protein was fused to dCas9 or dCas9–VP64. A previous study[35] showed that the repeat:antirepeat duplexes and stem loop 1 of sgRNA are essential for Cas9–sgRNA complex formation and binding to target DNA. The stem loops 2 and 3 of sgRNA only further enhance the stability of this complex, whereas the lack of these loops still causes Cas9 to fail in DNA interference. Consequently, the explanation of our results is that the aptamer–protein complex also reinforces the interaction between dCas9 and sgRNA and allows the dCas9 to function well in DNA binding with the help of the two remaining elements of sgRNA.

While we successfully constructed devices that responded to several ligands, extension of this platform to diverse signals may still be a problem. To achieve effective conformational change within the physiological concentration range, these studies require aptamer that binds its ligand with a high affinity. However, we usually need to alter the lower aptamer stem sequence or use a truncated sequence to constitute the antisense stem in the design of riboswitch, which may reduce the aptamers' binding strength. Therefore, future work should focus on selecting simple structured aptamer which shows a comparably high affinity after modification of the lower stem.

Despite the reported off-target effects of CRISPR–Cas9, recent examples outlining sgRNA design[36,37] or Cas9 (ref. 38) engineering can be used to improve specificity. dCas9 fused to newer repression or activation domains[39–41] may also achieve more robust gene repression or activation and modulate gene expression levels within a broad range of efficiencies. On the basis of further ensuring specificity and efficiency, the ability to edit cell signaling may have many powerful applications in biotechnology and medicine.

METHODS

Methods and any associated references are available in the online version of the paper.

Note: Any Supplementary Information and Source Data files are available in the online version of the paper.

ACKNOWLEDGMENTS

We are indebted to the donors whose names were not included in the author list, but who participated in this program. This work was supported by the National Key Basic Research Program of China (973 Program) (2014CB745201 to Z.C.), National Natural Science Foundation of China (81402103 to Y.L.), the Shenzhen Municipal Government of China (ZDSYS201504301722174,

© 2016 Nature America, Inc. All rights reserved.

JCYJ20150330102720130 and GJHZ20150316154912494 to W.H.), Special Support Funds of Shenzhen for Introduced High-Level Medical Team to W.H., and Shenzhen High Level Medical Discipline Development Program (2016031638 to W.H. and Z.C.).

AUTHOR CONTRIBUTIONS

Y.L., Y.Z., Z.C., A.H., J.L., H.W., L.L., C.Z., J.L., X.G. and Q.Z. performed experiments and data analysis. Y.L., W.H. and Z.C. designed and supervised the project and wrote the paper. W.H. and Z.C. provided financial support for the project.

COMPETING FINANCIAL INTERESTS

The authors declare no competing financial interests.

Reprints and permissions information is available online at http://www.nature.com/reprints/index.html.

1. Scott, J.D. & Pawson, T. Cell signaling in space and time: where proteins come together and when they're apart. *Science* **326**, 1220–1224 (2009).
2. Riento, K. & Ridley, A.J. Rocks: multifunctional kinases in cell behaviour. *Nat. Rev. Mol. Cell Biol.* **4**, 446–456 (2003).
3. Bhattacharyya, R.P., Reményi, A., Yeh, B.J. & Lim, W.A. Domains, motifs, and scaffolds: the role of modular interactions in the evolution and wiring of cell signaling circuits. *Annu. Rev. Biochem.* **75**, 655–680 (2006).
4. Slusarczyk, A.L., Lin, A. & Weiss, R. Foundations for the design and implementation of synthetic genetic circuits. *Nat. Rev. Genet.* **13**, 406–420 (2012).
5. Youk, H. & Lim, W.A. Secreting and sensing the same molecule allows cells to achieve versatile social behaviors. *Science* **343**, 1242782 (2014).
6. Townshend, B., Kennedy, A.B., Xiang, J.S. & Smolke, C.D. High-throughput cellular RNA device engineering. *Nat. Methods* **12**, 989–994 (2015).
7. Chau, A.H., Walter, J.M., Gerardin, J., Tang, C. & Lim, W.A. Designing synthetic regulatory networks capable of self-organizing cell polarization. *Cell* **151**, 320–332 (2012).
8. Galloway, K.E., Franco, E. & Smolke, C.D. Dynamically reshaping signaling networks to program cell fate via genetic controllers. *Science* **341**, 1235005 (2013).
9. Hsu, P.D., Lander, E.S. & Zhang, F. Development and applications of CRISPR-Cas9 for genome engineering. *Cell* **157**, 1262–1278 (2014).
10. Qi, L.S. *et al.* Repurposing CRISPR as an RNA-guided platform for sequence-specific control of gene expression. *Cell* **152**, 1173–1183 (2013).
11. Maeder, M.L. *et al.* CRISPR RNA-guided activation of endogenous human genes. *Nat. Methods* **10**, 977–979 (2013).
12. Mali, P. *et al.* CAS9 transcriptional activators for target specificity screening and paired nickases for cooperative genome engineering. *Nat. Biotechnol.* **31**, 833–838 (2013).
13. Zalatan, J.G. *et al.* Engineering complex synthetic transcriptional programs with CRISPR RNA scaffolds. *Cell* **160**, 339–350 (2015).
14. Polstein, L.R. & Gersbach, C.A. A light-inducible CRISPR-Cas9 system for control of endogenous gene activation. *Nat. Chem. Biol.* **11**, 198–200 (2015).
15. Nihongaki, Y., Yamamoto, S., Kawano, F., Suzuki, H. & Sato, M. CRISPR-Cas9-based photoactivatable transcription system. *Chem. Biol.* **22**, 169–174 (2015).
16. Boerneke, M.A. & Hermann, T. Ligand-responsive RNA mechanical switches. *RNA Biol.* **12**, 780–786 (2015).
17. Bayer, T.S. & Smolke, C.D. Programmable ligand-controlled riboregulators of eukaryotic gene expression. *Nat. Biotechnol.* **23**, 337–343 (2005).
18. Culler, S.J., Hoff, K.G. & Smolke, C.D. Reprogramming cellular behavior with RNA controllers responsive to endogenous proteins. *Science* **330**, 1251–1255 (2010).
19. Moon, T.S., Lou, C., Tamsir, A., Stanton, B.C. & Voigt, C.A. Genetic programs constructed from layered logic gates in single cells. *Nature* **491**, 249–253 (2012).
20. Green, C. *Restore Wild-Type Functions to P53 Mutants Using an RNA-Based Combinatorial Approach*. Report No. DAMD17-97-1-7036 (SRI International, 2000).
21. Zhao, X. *et al.* An RNA aptamer that interferes with the DNA binding of the HSF transcription activator. *Nucleic Acids Res.* **34**, 3755–3761 (2006).
22. Jian, Y. *et al.* RNA aptamers interfering with nucleophosmin oligomerization induce apoptosis of cancer cells. *Oncogene* **28**, 4201–4211 (2009).
23. Tsui, K.H., Cheng, A.J., Chang, Pe., Pan, T.L. & Yung, B.Y. Association of nucleophosmin/B23 mRNA expression with clinical outcome in patients with bladder carcinoma. *Urology* **64**, 839–844 (2004).
24. Kaur, J. & Tikoo, K. Ets1 identified as a novel molecular target of RNA aptamer selected against metastatic cells for targeted delivery of nano-formulation. *Oncogene* **34**, 5216–5228 (2015).
25. Xu, W. & Ellington, A.D. Anti-peptide aptamers recognize amino acid sequence and bind a protein epitope. *Proc. Natl. Acad. Sci. USA* **93**, 7475–7480 (1996).
26. Lee, Y.J. & Lee, S.W. Regression of hepatocarcinoma cells using RNA aptamer specific to alpha-fetoprotein. *Biochem. Biophys. Res. Commun.* **417**, 521–527 (2012).
27. Luo, X., Budihardjo, I., Zou, H., Slaughter, C. & Wang, X. Bid, a Bcl2 interacting protein, mediates cytochrome c release from mitochondria in response to activation of cell surface death receptors. *Cell* **94**, 481–490 (1998).
28. Beisel, C.L., Bayer, T.S., Hoff, K.G. & Smolke, C.D. Model-guided design of ligand-regulated RNAi for programmable control of gene expression. *Mol. Syst. Biol.* **4**, 224 (2008).
29. An, C.I., Trinh, V.B. & Yokobayashi, Y. Artificial control of gene expression in mammalian cells by modulating RNA interference through aptamer-small molecule interaction. *RNA* **12**, 710–716 (2006).
30. Wittmann, A. & Suess, B. Engineered riboswitches: expanding researchers' toolbox with synthetic RNA regulators. *FEBS Lett.* **586**, 2076–2083 (2012).
31. Winkler, W., Nahvi, A. & Breaker, R.R. Thiamine derivatives bind messenger RNAs directly to regulate bacterial gene expression. *Nature* **419**, 952–956 (2002).
32. Yen, L. *et al.* Exogenous control of mammalian gene expression through modulation of RNA self-cleavage. *Nature* **431**, 471–476 (2004).
33. Chen, Y.Y., Jensen, M.C. & Smolke, C.D. Genetic control of mammalian T-cell proliferation with synthetic RNA regulatory systems. *Proc. Natl. Acad. Sci. USA* **107**, 8531–8536 (2010).
34. Shechner, D.M., Hacisuleyman, E., Younger, S.T. & Rinn, J.L. Multiplexable, locus-specific targeting of long RNAs with CRISPR-Display. *Nat. Methods* **12**, 664–670 (2015).
35. Nishimasu, H. *et al.* Crystal structure of Cas9 in complex with guide RNA and target DNA. *Cell* **156**, 935–949 (2014).
36. Fu, Y., Sander, J.D., Reyon, D., Cascio, V.M. & Joung, J.K. Improving CRISPR-Cas nuclease specificity using truncated guide RNAs. *Nat. Biotechnol.* **32**, 279–284 (2014).
37. Doench, J.G. *et al.* Optimized sgRNA design to maximize activity and minimize off-target effects of CRISPR-Cas9. *Nat. Biotechnol.* **34**, 184–191 (2016).
38. Slaymaker, I.M. *et al.* Rationally engineered Cas9 nucleases with improved specificity. *Science* **351**, 84–88 (2016).
39. Thakore, P.I. *et al.* Highly specific epigenome editing by CRISPR-Cas9 repressors for silencing of distal regulatory elements. *Nat. Methods* **12**, 1143–1149 (2015).
40. Hilton, I.B. *et al.* Epigenome editing by a CRISPR-Cas9-based acetyltransferase activates genes from promoters and enhancers. *Nat. Biotechnol.* **33**, 510–517 (2015).
41. Gilbert, L.A. *et al.* Genome-scale CRISPR-mediated control of gene repression and activation. *Cell* **159**, 647–661 (2014).

© 2016 Nature America, Inc. All rights reserved.

ONLINE METHODS

Design principles for the signal conductors. We implemented five engineering design principles in constructing these devices: (i) sensibility (devices that efficiently sense and respond to one specific biological signal); (ii) conductibility (devices that effectively activate or inactivate expression of the targeted gene in the presence of the desired signal); (iii) flexibility (devices that allow dose-dependent control of gene expression over a dynamic range); (iv) extensibility (devices that synergistically integrate multiple signals to simultaneously tune the expression patterns of various other genes) and (v) universality (functional devices that are independent of cell-specific mechanisms).

Plasmid construction. The plasmid vectors pcDNA–dCas9–HA (plasmid no. 61355, Addgene) and M–SPn–VP64 (plasmid no. 48674, Addgene) were used to transiently express inactive Cas9 protein and Cas9–VP64 fusion protein, respectively, in mammalian cells. The original sgRNAs were designed using the online design tool "CRISPR-ERA" (http://CRISPR-ERA.stanford.edu). The designed cDNA sequence for each reprogrammed sgRNA was synthesized and inserted into pGPU6/GFP/Neo vector digested with BamHI/Bbs I. The RNA secondary structures and RNA free energies of the designed sgRNAs are shown in **Supplementary Figure 35**. The cDNA sequences of mutated aptamers used for construction of negative controls are shown in **Supplementary Table 3**. To construct plasmids pcDNA3–MS2–dCas9 and pcDNA3–Rev–dCas9–VP64, cDNA sequences for MS2–dCas9 and Rev–dCas9–VP64 genes were inserted into pcDNA3 at restriction sites of BamHI/EcoRI, respectively. To construct plasmids Tk-NF-κB and Tk-β-catenin, cDNA sequences for NF-κB and β-catenin were inserted into pRL-TK vector digested with CspI/XbaI. shRNA expression vectors for targeting p21, p53, NPM, E-cadherin, Ets-1, NF-κB, β-catenin and AFP were constructed by inserting the related cDNA sequences into pLKO.1 puro vector (plasmid no. 8453, Addgene) digested with AgeI/EcoRI.

Surface plasmon resonance assay. We used a Biacore X100 instrument (GE Healthcare, Uppsala, Sweden) for surface plasmon resonance experiments. Briefly, the CM5 sensor chip (GE Healthcare) was pre-equilibrated with running buffer (10 mM HEPES, pH 7.5, 150 mM NaCl, 1 mM $MgCl_2$, 1 mM $CaCl_2$ and 2.7 mM KCl) before immobilization of ligands onto the chip surface and activated with 0.05 M N-hydroxysuccinimide (NHS; GE Healthcare) and 0.2 M 1-ethyl-3-(3-dimethylaminopropyl) carbodiimide (EDC; GE Healthcare). Each ligand (small molecule or protein) was then injected into the flow cells of the sensor chip, and amine-coupling chemistry was used for covalently attaching ligands to the sensor chip surface. After immobilization of the ligand, the chip surface was deactivated with 1 M ethanolamine hydrochloride to block the remaining unreacted groups. DNA template oligonucleotides for sgRNAs were transcribed into RNA *in vitro* using the MEGA-shortscript T7 kit (Life Technologies). Then, various concentrations of the sgRNAs were injected over the sensor surface for 1.5 min at 5 μl/min and subsequently analyzed for equilibrium binding properties. An example for calculating the equilibrium dissociation constant (K_D) was shown in **Supplementary Figure 36**. Binding affinities of various reprogrammed sgRNAs and the mutated controls were shown in **Supplementary Table 5**.

Cell culture and cell transfection. HEK-293T, 5637, T24, HepG2, ACHN, WRL-68 and SV-HUC1 cell lines, known for high transfection efficiency and wide dynamic range of expression, were purchased from American Type Culture Collection (ATCC) and maintained in DMEM medium supplemented with 10% fetal bovine serum (Invitrogen) in the presence of 5% CO2 at 37 °C in incubator. For transient transfection experiments, cells were treated with the mixtures of plasmids using Lipofectamine 2000 Transfection Reagent (Invitrogen, Carlsbad, CA, USA) according to manufacturer's protocols after they reached 70–80% confluency. For transfections involving gene regulation, cell migration and cell apoptosis, 350,000 cells were seeded in 12-well plates the day before transfection. For transfections involving cell proliferation, 5,000 cells per well were seeded in 96-well plates the day before transfection. Transfection efficiency in each sample was estimated according to the percentage of GFP positive cells, in which GFP was expressed from the plasmid pGPU6–GFP–Neo vector, regulated by the stable viral CMV promoter.

RNA extraction and real-time quantitative PCR. The TRIzol reagent (Invitrogen, Grand Island, NY, USA) was used to extract total RNA from cells transfected with the plasmids according to manufacturer's protocols. Total RNA was transformed to cDNA using RevertAid First Strand cDNA Synthesis Kit (Fermentas, Hanover, MD, USA) according to the related protocols. The reactions of real-time quantitative PCR were performed on an ABI PRISM 7000 Fluorescent Quantitative PCR System (Applied Biosystems, Foster City, CA, USA) using All-in-One qPCR Mix (GeneCopoiea Inc., Rockville, MD, USA). The PCR cycling parameters used were as follows: 95 °C for 15 min, followed by 40 cycles of 94 °C for 15 s, 55 °C for 30 s and 72 °C for 30 s. GAPDH was used as the internal control, and the data were normalized to the expression of GAPDH. Relative gene expression was calculated using the Delta-Delta-Ct (ddCt) algorithm. The reported values are the average of five biological replicates ± s.d.

ELISA assay of VEGF concentration. The concentration of VEGF protein was measured by ELISA assay according to the manufacturer's protocols. Briefly, 10^6 sample cells were harvested, and the supernatants of cellular lysates were collected by centrifugation. The VEGF protein was quantified using a colorimetric reaction, and the optical density (OD value) of the end product was calculated using a microplate reader (Bio-Rad, Hercules, CA, USA). Then the values of OD were converted to protein concentrations through the standard curves. Each experiment was performed five times.

Luciferase assay. Relative Renilla luciferase activity was detected by the Dual-Luciferases Reporter Assay kit (Promega E1980) using a Multimode Detector (Beckman Coulter, CA, USA) according to manufacturer's instructions at 48 h post-transfection. The assays were performed in duplicate and the experiments were repeated five times.

Cell proliferation assay. Cell proliferation was monitored using CCK-8 assay according to the manufacturer's instructions. Cells were seeded in a 96-well plate for 24 h and then transiently transfected with the plasmids. At 0, 24, 48 or 72 h post-transfection, 10 μl of CCK-8 reagent was added to each well, and the cells were incubated for 1 h. Absorbance was calculated at a wavelength of

© 2016 Nature America, Inc. All rights reserved.

doi:10.1038/nmeth.3994

450 nm via using a microplate reader (Bio-Rad, Hercules, CA, USA). The assays were repeated five times independently.

Cell migration assay. Cell migration was determined by the wound-healing assay. Briefly, cells were seeded in 12-well plates at equal density and grown to 90% confluency. A clean line was created by using a sterile 200 µl pipette tip at 5 h post-transfection. Areas of wound were marked and photographed with a digital camera system at 0 h and 20 h. Cell migration distance (mm) was calculated by the software HMIAS-2000. Each experiment was repeated five times.

Cell apoptosis assay. At 48 h post-transfection, the Hoechst 33258 staining kit (Life, Eugene, OR, USA) was used to observe the apoptotic cells induced by signal conductors. Briefly, the cancer cells were fixed in 4% paraformaldehyde for 10 min and washed twice in PBS. Then, the cells were stained with 0.5 ml of Hoechst 33258 staining for 5 min, and photos were taken under a fluorescence microscope at a wavelength of 350 nm. Each assay was carried out five times.

Western blot analysis. Cells were washed in PBS and lysed in RIPA buffer. The protein concentration was determined using the BCA protein assay. Equal amounts of whole-protein extract were electrophoresed onto SDS–polyacrylamide gels and then transferred to PVDF membranes (Millipore, Billerica, MA, USA). Samples were blocked in 5% dry milk and incubated overnight with the primary antibodies (Abcam, Cambridge, MA, USA) against NF-κB (ab32536; 1:1,000), p53 (ab1101; 1:5,000), HSF1 (ab61382; 1:1,000), β-catenin (ab16051; 1:5,000), NPM (ab10530; 1:5,000), E-cadherin (ab1416; 1:1,000), Ets-1 (ab96478; 1:2,000), BCL2 (ab32124; 1:1,000), BAX (ab32503; 1:10,000) and AFP (ab133617; 1:2,000). Then, the samples were incubated with horseradish-peroxidase-conjugated secondary antibody (Amersham, Piscataway, NJ, 1 µg/ml). Finally, the immunoblots were developed with Super Signal chemiluminescence reagents (Pierce Chemical).

***In vitro* detection of GFP-expressing cell lines.** The cells were cultured for 24 h and transfected with signal conductor or negative control. The cells were then examined for GFP expression after 24 h using fluorescent microscopy (MicroPublisher 3.3 RTV; Olympus, Japan), and the images were taken in autoexposure mode.

Enzyme-linked immunosorbent assay. The cell apoptosis was detected through calculating histone-complexed DNA fragments (nucleosomes) in cytoplasm with cell death detection ELISA (Roche Applied Science) according to the instructions. The absorbance was measured at 405 nm wavelength by a microplate reader (Bio-Rad), and its value was proportional to the amount of nucleosomes released into the cytoplasm. Each assay was carried out five times.

Tumor development assay in nude mouse model. All experiments involving animals were approved by Institutional Ethics Review Board. In detail, 10^7 HepG2/T24/ACHN cells were suspended in 100 µl PBS and injected subcutaneously into the right armpits of three 4-week-old female BALB/c nude mice. Random animals were assigned to each treatment group. Intratumoral injections of 30 µg of either circuit-expressing plasmids (treatment groups) or negative-control-expressing plasmids (control groups) were given every 3 d after the tumors were observed. Tumor growth was monitored over a 3-week period, and tumor volumes were calculated using the formula: $0.5 \times \text{length} \times \text{width}^2$. At the end of the experiment, mice were euthanized, and the subcutaneous weight of each tumor was measured.

Statistical analyses. No statistical methods were used to predetermine sample size. The investigators were blinded to allocation during experiments and outcome assessment. Statistical analysis was conducted using *t*-test or ANOVA, and $P < 0.05$ was considered statistically significant. All statistical tests were performed by using SPSS version 17.0 software (SPSS, Chicago, IL, USA).

Data availability. Plasmids sequences are listed in **Supplementary Tables 2** and **4**. Plasmids are available upon request.

© 2016 Nature America, Inc. All rights reserved.